Acta Oceanol. Sin., 2021, Vol. 40, No. 5, P. 47–57
https://doi.org/10.1007/s13131-021-1733-2
http://www.hyxb.org.cn
E-mail: ocean2@hyxb.org.cn

Revisiting ENSO impacts on the Indian Ocean SST based on a combined linear regression method

Lianyi Zhang[1, 2, 3, 4], Yan Du[1, 2, 3]*, Tomoki Tozuka[4, 5], Shoichiro Kido[5]

[1] State Key Laboratory of Tropical Oceanography, South China Sea Institute of Oceanology, Chinese Academy of Sciences, Guangzhou 510301, China

[2] University of Chinese Academy of Sciences, Beijing 100049, China

[3] Southern Marine Science and Engineering Guangdong Laboratory (Guangzhou), Guangzhou 511458, China

[4] Department of Earth and Planetary Science, Graduate School of Science, The University of Tokyo, Tokyo 113-0033, Japan

[5] Application Laboratory (APL), Research Institute for Value-Added-Information Generation (VAiG), Japan Agency for Marine-Earth Science and Technology, Yokohama 236-0001, Japan

Received 8 May 2020; accepted 30 June 2020

Abstract

The El Niño-Southern Oscillation (ENSO) has great impacts on the Indian Ocean sea surface temperature (SST). In fact, two major modes of the Indian Ocean SST namely the Indian Ocean Basin (IOB) and the Indian Ocean Dipole (IOD) modes, exerting strong influences on the Indian Ocean rim countries, are both influenced by the ENSO. Based on a combined linear regression method, this study quantifies the ENSO impacts on the IOB and the IOD during ENSO concurrent, developing, and decaying stages. After removing the ENSO impacts, the spring peak of the IOB disappears along with significant decrease in number of events, while the number of events is only slightly reduced and the autumn peak remains for the IOD. By isolating the ENSO impacts during each stage, this study reveals that the leading impacts of ENSO contribute to the IOD development, while the delayed impacts facilitate the IOD phase switch and prompt the IOB development. Besides, the decadal variations of ENSO impacts are various during each stage and over different regions. These imply that merely removing the concurrent ENSO impacts would not be sufficient to investigate intrinsic climate variability of the Indian Ocean, and the present method may be useful to study climate variabilities independent of ENSO.

Key words: Indian Ocean, ENSO, sea surface temperature, climate modes, combined linear regression

Citation: Zhang Lianyi, Du Yan, Tozuka Tomoki, Kido Shoichiro. 2021. Revisiting ENSO impacts on the Indian Ocean SST based on a combined linear regression method. Acta Oceanologica Sinica, 40(5): 47–57, doi: 10.1007/s13131-021-1733-2

1 Introduction

The El Niño-Southern Oscillation (ENSO) in the tropical Pacific is the strongest climatic phenomenon that has great impacts on the globe (Klein et al., 1999; McPhaden and Yu, 1999; Alexander et al., 2002; Cai et al., 2015). The Indian Ocean (IO), as one of being significantly affected area, draws many studies in recent decades because of its unique monsoon system and strong climatic influences on not only surrounding countries but also far regions (Ashok et al., 2001; Xie et al., 2002; Lau and Nath, 2004; Abram et al., 2008; Schott et al., 2009; Han et al., 2014). The ENSO has great impacts on the IO sea surface temperature (SST) that is usually considered as the energy source of the atmosphere and the proxy of climate variability at low latitudes (Meehl, 1993; Alexander et al., 2002; Annamalai et al., 2003; Ashok et al., 2003; Du et al., 2009; Chowdary et al., 2012). Based on the observations of SST, wind, and air-sea fluxes, previous studies have found two major climate modes in the tropical IO that are related with the ENSO, namely the Indian Ocean Basin (IOB) and the Indian Ocean Dipole (IOD) modes (Deser et al., 2010; Xie et al., 2016).

The IOB is characterized by basin-wide warming of SST anomalies during its positive phase, which is considered as the responses to the ENSO in the IO section (Klein et al., 1999; Yang et al., 2007; Du et al., 2009, 2013b). With an El Niño event, SST in the tropical IO warms up anomalously during boreal spring and summer through the ocean dynamics and ocean-atmosphere interactions, known as the capacitor effect (Xie et al., 2009). The IOB is stronger during ENSO-IOD co-occurrence years than during pure ENSO years (Chowdary and Gnanaseelan, 2007). During an El Niño, anti-cyclonic wind anomalies are induced over the southeastern IO, forcing a westward propagating downwelling Rossby wave and leading to positive SST anomalies in the southwestern tropical IO (Xie et al., 2009). Such SST warming further induces the northern IO warming via wind-evaporation-SST feedback in following spring (Xie and Philander, 1994), driving the IOB to mature phase (Du et al., 2009; Xie et al., 2009, 2016). The IOB can accelerate the El Niño demise in turn and affect climate variability in South Asia (Park et al., 2010; Chowdary et al.,

Foundation item: The National Natural Science Foundation of China under contract Nos 41830538 and 42090042; the Program of the Chinese Academy of Sciences under contract Nos 133244KYSB20190031, ZDRW-XH-2001902 and ISEE2018PY06; the Program of the Southern Marine Science and Engineering Guangdong Laboratory (Guangzhou) under contract Nos GML2019ZD0303 and 2019BT02H594.

*Corresponding author, E-mail: duyan@scsio.ac.cn

2019) and East Asia by inducing atmospheric Kelvin waves eastward into the western Pacific (Xie et al., 2009; Huang et al., 2010; Du et al., 2011), superimposing on intrinsic variability due to local air-sea interaction (Wang et al., 2020).

The positive IOD features a zonal gradient in the tropics with a see-saw structure of SST: anomalous SST cooling in the east and warming in the west. It generally matures in boreal autumn before an El Niño peak (Saji et al., 1999; Webster et al., 1999). A positive IOD event usually leads to drought in the Maritime Continent but flood in East Africa, causing large socioeconomic damages (Guan and Yamagata, 2003; Behera et al., 2008; Luo et al., 2008; Qiu et al., 2014; Du and Zhang, 2015). To some extent, the IOD can be induced by the ENSO because the ENSO affects the Indo-Pacific Walker Circulation and further induces wind anomalies in the equatorial IO (Annamalai et al., 2003; Fischer et al., 2005; Zheng et al., 2013; Yang et al., 2015; Stuecker et al., 2017). However, the IOD is known as an intrinsic climate mode of the IO without concurring ENSO (Du et al., 2013a; Guo et al., 2015; Sun et al., 2015; Wang et al., 2016; Crétat et al., 2017), and what triggers the independent IOD is a hot research topic at the beginning but remains an open question still.

Although it is well-known that the ENSO can influence the IO SST, it remains unclear how to quantify the ENSO impacts on the SST. Based on the observational data and statistical analyses, this study aims to answer this question by isolating ENSO-induced SST variations through a novel approach. This procedure would also benefit to study intrinsic variability in the IO.

2 Data and methods

The Extended Reconstructed Sea Surface Temperature (ERSST) version 5 data with a spatial resolution of 2°×2° in the period of 1950–2019 due to better data reliability of SST after the 1950s are used in this study (Huang et al., 2017). The seasonal cycle and long-term trend are firstly removed from the original data. The IOB index is defined as area-mean SST anomalies over the tropical IO (15°S–15°N, 40°–100°E), while the IOD index is defined as the difference between area-mean SST anomalies over the western tropical IO (10°S–10°N, 50°–70°E) and the southeastern tropical IO (10°S–0°, 90°–110°E). The Niño3.4 index is used to represent the ENSO and defined as area-mean SST anomalies over the central-eastern equatorial Pacific (5°S–5°N, 120°–170°W). Note that other datasets are also analyzed producing similar results, including the Met Office Hadley Centre's sea ice and sea surface temperature (HadISST) (Kennedy et al., 2011a, b), the Optimum Interpolation Sea Surface Temperature (OISST) (Reynolds et al., 2002), and the ERSST version 3b (Smith et al., 2008).

To isolate the ENSO impacts in the IO, a combined linear regression (CLR) is applied based on the notion that the ENSO is a dynamical entity and both developing and decaying stages of ENSO have considerable impacts on the IO (Penland and Matrosova, 2006; Xie et al., 2009; Compo and Sardeshmukh, 2010). A typical ENSO event usually starts to develop in boreal summer (June to August), peaks in winter (December to January of next year), and subsequently decays in spring (March–April) (Rasmusson and Carpenter, 1982). Considering this strong seasonality of the ENSO, a three-step recursive regression is conducted base on the following formula:

$$y_{i-1} = y_i + b_i x_i, \quad i = 1, 2, 3, \tag{1}$$

where y_i and b_i represent the intercept and the regression coefficient, respectively. In the first regression (i.e., i=1), a concurrent regression is applied upon the Niño3.4 index to the IO SST anomaly. The original IO SST anomaly is set as y_0 and the Niño3.4 index is set as x_1. The concurrent impacts of ENSO on the IO SST can be expressed as b_1x_1. The remaining part of the IO SST anomaly becomes y_1 (i.e., $y_0 - b_1x_1$). In the second recursive regression (i=2), x_2 is set as the bimonthly mean value of the Niño3.4 index in December of the ENSO developing year and in January of the decaying year (i.e., the typical peak stage of ENSO, also same as x_3); then x_2 is regressed onto y_1 in each month of the ENSO developing year. Again, y_2(i.e., $y_0 - b_1x_1 - b_2x_2$) represents the remaining part. In the third recursive regression, x_3 is similarly regressed onto y_2 monthly in the decaying year and obtain y_3. The second/third step is a kind of lead/lag regression that represents the ENSO impacts during the developing/decaying stage. At the end of this recursive regression, y_3 represents the IO SST anomaly after removing all the ENSO impacts, while the sum of b_ix_i represents the ENSO contribution to the IO SST anomaly. A time-window of 12-year for running regression is set to avoid the interference of the ENSO decadal variability with the CLR results. A students' t test at the 80% confidence level is used to exclude fragile ENSO impacts (Bretherton et al., 1999). Due to the limitation of lead-lag regressions, the period of 1951–2018 is retained to ensure the removal of ENSO cycles near the end points. Note that even though it has considered the ENSO impacts during different periods, the CLR is still based on the linear concept and may miss non-linear effects of the ENSO. Other potential issues are addressed in Discussion.

3 Results

Here, a classic method, the empirical orthogonal function (EOF) analysis, is used to extract the SST modes in the IO and compare each principal component (PC) with the Niño3.4 index. The decomposition of the original data is consistent with previous studies (Deser et al., 2010), in which the basin-wide warming pattern explains major part of the IO SST variability (23.0%), while the second mode exhibits a zonal dipole structure (14.5%) (Figs 1a and b). Both PC1 and PC2 show good correlations with the Niño3.4 index in a 24-month lead-lag window (Fig. 2a). Besides, PC1 leads PC2 by 6-month or lags by 4-month (Fig. 2b). This is consistent with the fact that accompanied by an El Niño development the IO firstly responds in the form of the zonal gradient of SST anomalies, and when the El Niño decays, basin-wide SST warms up. Moreover, an El Niño is usually followed by a La Niña, which suggests that there would be a negative IOD forced by a La Niña event in the El Niño decaying year.

One usual way to remove the ENSO impacts is by subtracting concurrent regression. However, such approach cannot totally isolate the ENSO impacts, because the ENSO has considerable effects even before and after its mature phase (Fig. 2a) (Penland and Matrosova, 2006). In comparison, the CLR can cover the leading and delayed impacts of ENSO. The EOF decompositions onto the ENSO-removed data by two methods exhibit clear differences. When only the concurrent impact is removed, the EOF1 still shows a uniform SST anomaly pattern like the original results but with lower variance (20.1%), while the EOF2 is almost unchanged (Figs 1c and d). The lead-lag correlations between PC and Niño3.4 prove that the ENSO signals are retained in the IO (Figs 2c and d).

On the other hand, the EOF1 of the CLR results (16.5%) shows that the core of SST anomalies is anchored at the southern IO, and only very weak SST anomalies are found in the tropical IO (Fig. 1e). The EOF2 (14.4%) is still a dipole pattern, but closer to the Indian Ocean Subtropical Dipole pattern with a southwest-

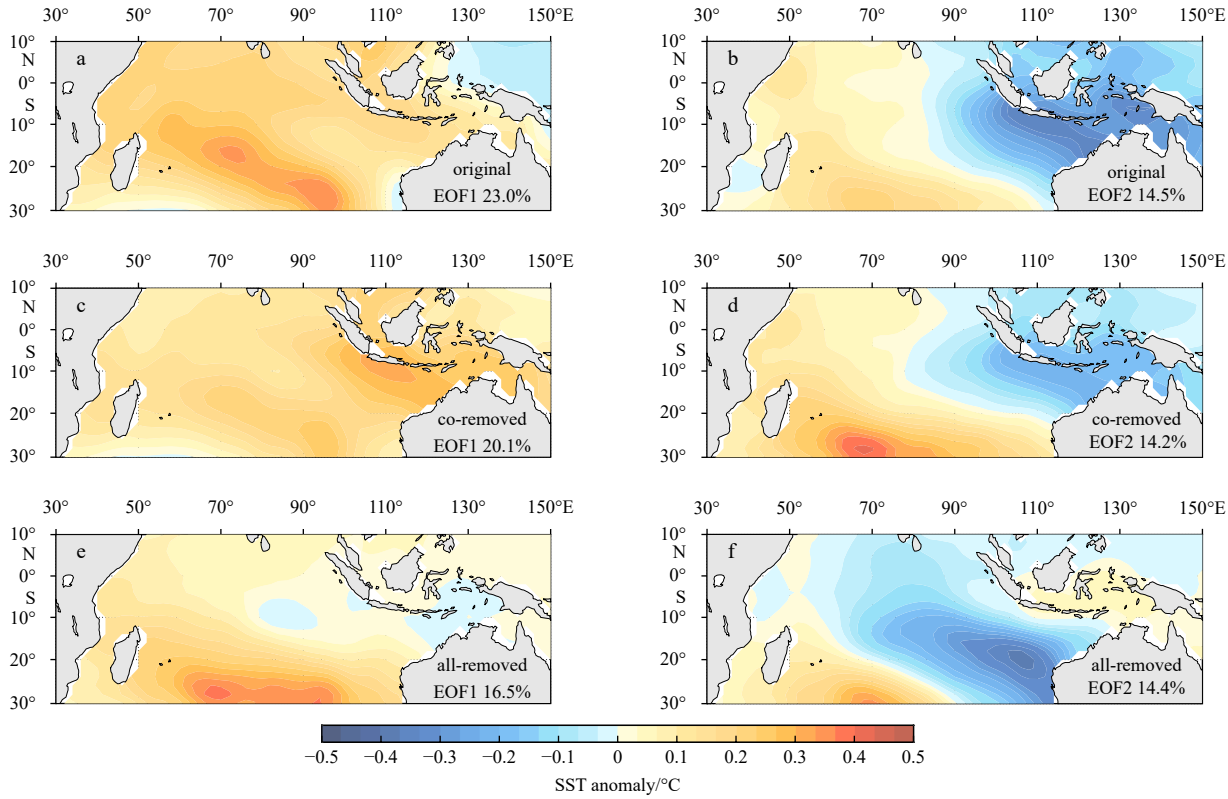

Fig. 1. Spatial patterns of the first two modes of the empirical orthogonal function (EOF) onto original sea surface temperature (SST) anomalies (a, b), SST anomalies without the concurrent impact of the El Niño-Southern Oscillation (ENSO) (c, d), and SST anomalies without all ENSO impacts derived by the combined linear regression (CLR) in the Indian Ocean (IO) (e, f).

northeast orientation (Fig. 1f) (Behera and Yamagata, 2001; Suzuki et al., 2004; Morioka et al., 2012). After applying the CLR, the spatial patterns of EOF modes change more than those derived by the usual concurrent regression. In addition, the correlations of the first two PCs with the ENSO reduce significantly (Fig. 2e). The mutual relationship between two leading modes is retained, which possibly suggests a connection between the tropical and subtropical IO SST. Note that the relationship between the IOD and the IOB becomes much weaker after removing the ENSO impacts (not shown) than that with the ENSO impacts (Fig. 2b). This also suggests that the ENSO plays an important role in the apparent IOD-IOB link.

The root-mean-square (RMS) distribution of SST anomaly is used to better display the ENSO impacts for all and each stage obtained by the CLR. Figures 3a and b exhibit original and ENSO-removed results, while Figure 3c is the difference between above two, which indicates the ENSO-induced SST variation. The ENSO-induced signals are mainly in the western tropical IO (Box A), the southeastern tropical IO (Box B), the southern IO (Box C), and the region west of Australia (Box D). Regarding each stage, the concurrent impact mainly contributes to the IOB (Boxes A and C) and Ningaloo Niño/Niña (Box D) modes (Feng et al., 2013; Tozuka et al., 2014; Zhang et al., 2018c), while the leading and delayed impacts concentrate more on the southeastern tropical IO (Box B), which would influence the IOD most significantly.

Since the IOB and the IOD are the first two leading modes of IO SST (Fig. 1), the indices of IOB and IOD are set as proxies to evaluate the ENSO influences. Figure 4 shows the indices with trimonthly-means during respective mature phases (February–April for the IOB and August–October for the IOD). Before applying the CLR, several remarkable cases of two modes that co-occurred with El Niño can be observed, such as the 1982/83, 1997/98 and 2015/16 events. After removing the ENSO impacts, the IOB index decreases significantly. The number of positive IOB events decreases by about 83% (from 12 to 2, Fig. 4a), while the decrease is only 25% for positive IOD events (from 12 to 9, Fig. 4c). In addition, RMS of the whole time series of the IOB and the IOD indices decrease by 36.9% (from 0.23°C to 0.15°C) and 12.6% (from 0.40°C to 0.35°C), respectively. These imply that the IOB is more strongly tied to the ENSO occurrence compared to the IOD. The comparison between ENSO-induced IOB and original IOB shows the ENSO contributes largely to the IOB seasonality, with the intensity of 0.22°C vs. 0.27°C in their peak phases (Fig. 4b). Without the ENSO impacts, the spring peak of the IOB disappears and the intensity is almost constant at about 0.15°C throughout the year (Fig. 4b). Therefore, without the ENSO impacts, ENSO-related processes including downwelling Rossby waves in the southern IO and heat flux anomalies in the northern IO are significantly reduced and the number of IOB events decreases. Although the IOB is known as the ENSO-forced phenomenon, there are some positive IOB events occurring under a weak El Niño condition (e.g., 1970, 1991). Some even survive after removing the ENSO impacts, suggesting that there may be a few IOB events induced by internal variability, e.g., internal Rossby waves in the southern IO (Masumoto and Meyers, 1998; Gnanaseelan and Vaid, 2009), which awaits further studies.

In contrast, responses to the ENSO are quite different for the IOD. Although the southeasterly wind anomalies associated with the El Niño over the eastern equatorial IO can trigger the positive

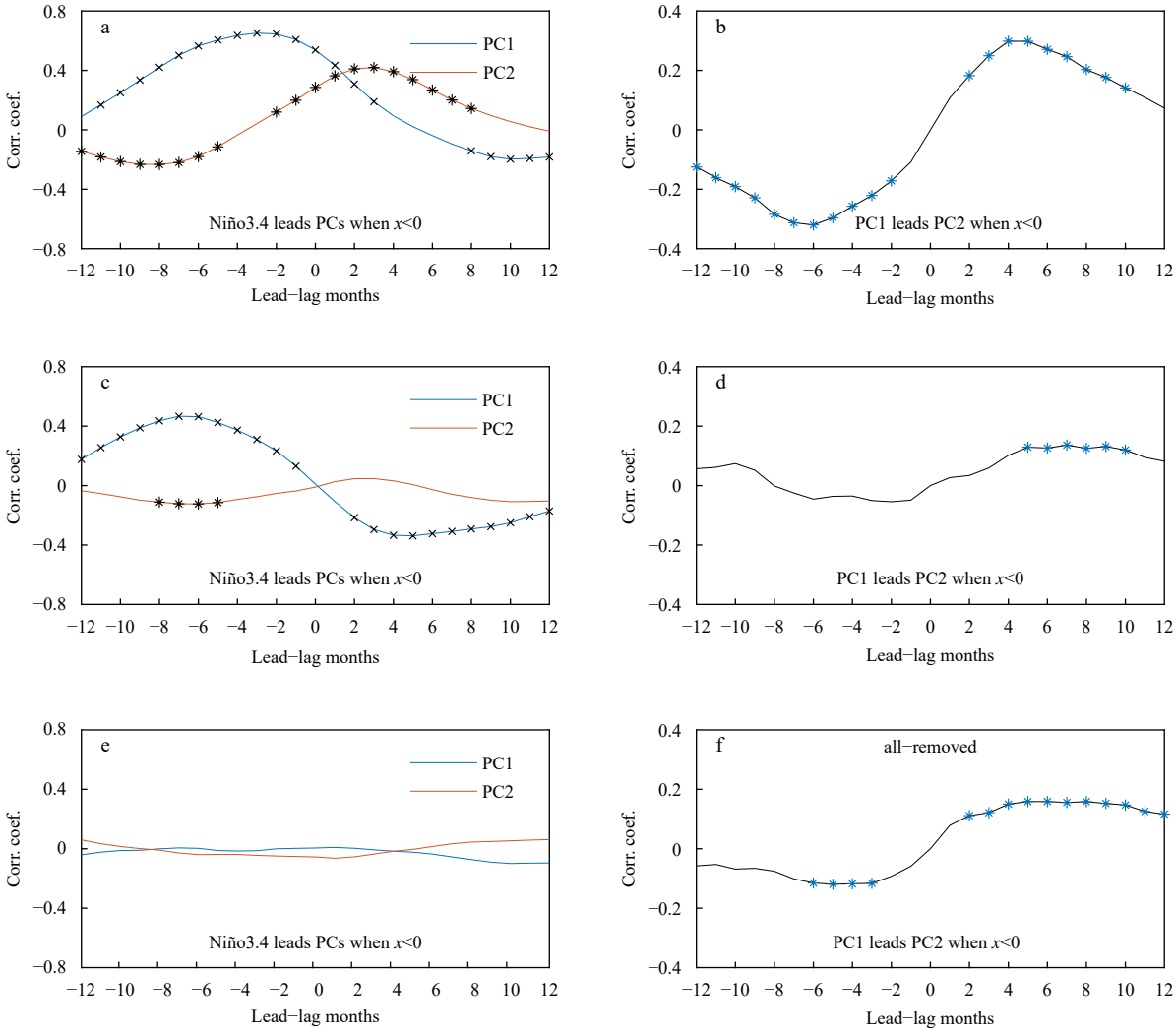

Fig. 2. Lead-lag correlation coefficients between the principal components (PCs) for the first two EOF modes of original SST anomalies and the Niño3.4 index (a). c and e as in a, but with the concurrent and all ENSO impacts removed by the CLR, respectively. b, d and f as in a, c and e, but for lead-lag correlation coefficients between the first two PCs. Correlation coefficients exceeding the 99% confidence level of students' *t* test are marked by "×" or "*".

IOD event, the IOD is not weakened as much as the IOB since the IOD can independently occur with intrinsic variability of the IO. For example, without the ENSO impacts, the 1997 positive IOD event disappears, but the 2015 event just weakens slightly, implying other mechanism at work (Zhang et al., 2018b). Other strong IOD events, such as the 1961, 1994 and 2006 events, are merely affected by application of the CLR as the El Niño are weak or even absent during these years (Vinayachandran et al., 1999; Horii et al., 2008). Moreover, the IOD usually develops from boreal summer and peaks in autumn, as the ENSO contributes to the strong peak during September–November. Although the intensity becomes weaker without the ENSO impacts, the IOD still shows a phase lock to boreal autumn with a slight shift in the peak month from October (0.57°C) to September (0.44°C) (Fig. 4d). This agrees with previous model studies (Behera et al., 2006; Yang et al., 2015). The above results suggest that the IOD is independent from the ENSO, but partly influenced by the ENSO especially during the IOD mature phase.

4 Discussion

Compared with the traditional regression method to exclude the ENSO signals, which only removes the concurrent part, the CLR can take account of the leading and delayed ENSO impacts. It is important to clarify why it is necessary to exclude impacts from these two periods. In particular, it is not clear how the ENSO can exert influences beforehand.

First, evolutions of the IOD and the IOB do not perfectly align with the ENSO. The ENSO tends to develop since boreal summer (sometimes earlier) (Xu and Chan, 2001), peak in winter, and decay during following spring. However, the IOD develops in summer and autumn earlier than the ENSO (Du et al., 2013a), whereas the IOB develops during spring of the ENSO decaying year (Fig. 2a) (Xie et al., 2009). These time differences imply that the concurrent regression cannot totally capture the ENSO impacts on the IO SST.

In addition, interactions between the IO SST and the ENSO are important (Yu et al., 2002; Ashok et al., 2003; Behera and Yamagata, 2003; Annamalai et al., 2005; Kug et al., 2006; Luo et al., 2010; Zhao et al., 2016; Zhang et al., 2018a). Not only the ENSO can induce the IOD and the IOB, but also the IOD and the IOB in turn can affect the ENSO evolution (Annamalai et al., 2010; Santoso et al., 2012) or transition (Izumo et al., 2010; Yuan et al.,

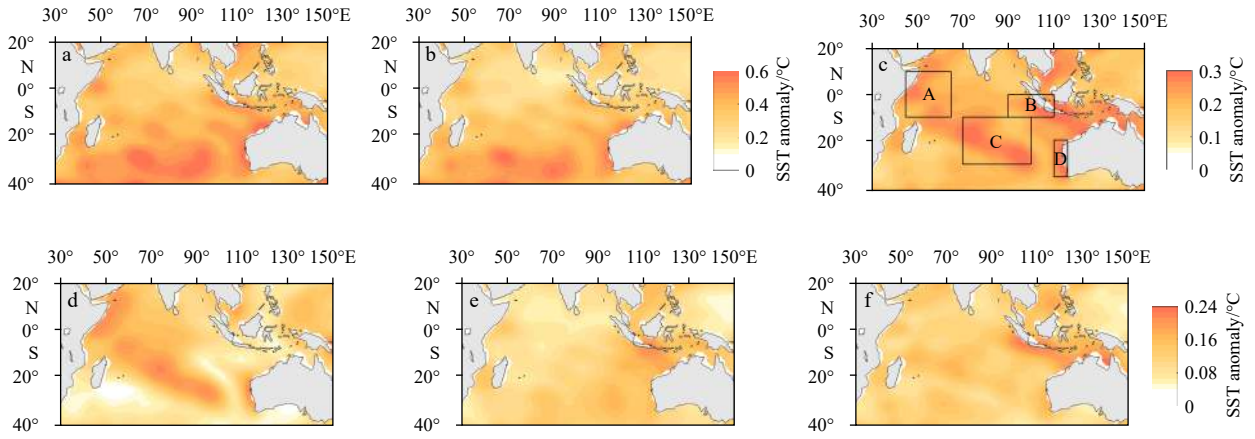

Fig. 3. Root-mean-square (RMS) of SST anomalies in the Indian Ocean (IO). a. Original SST anomalies, b. SST anomalies without all ENSO impacts, c. ENSO-induced SST anomalies, and d–f. ENSO-induced SST anomalies during the ENSO concurrent, developing, and decaying stages, respectively. Boxes A, B, C and D indicate four high RMS value regions over the western tropical IO (10°S–10°N, 45°–65°E), the southeastern tropical IO (10°S–0°, 90°–110°E), the southern IO (10°–30°S, 70°–100°E), and the region west of Australia (20°–35°S, 110°–116°E). Note that the range of colorbar decreases gradually from the upper to the lower panels.

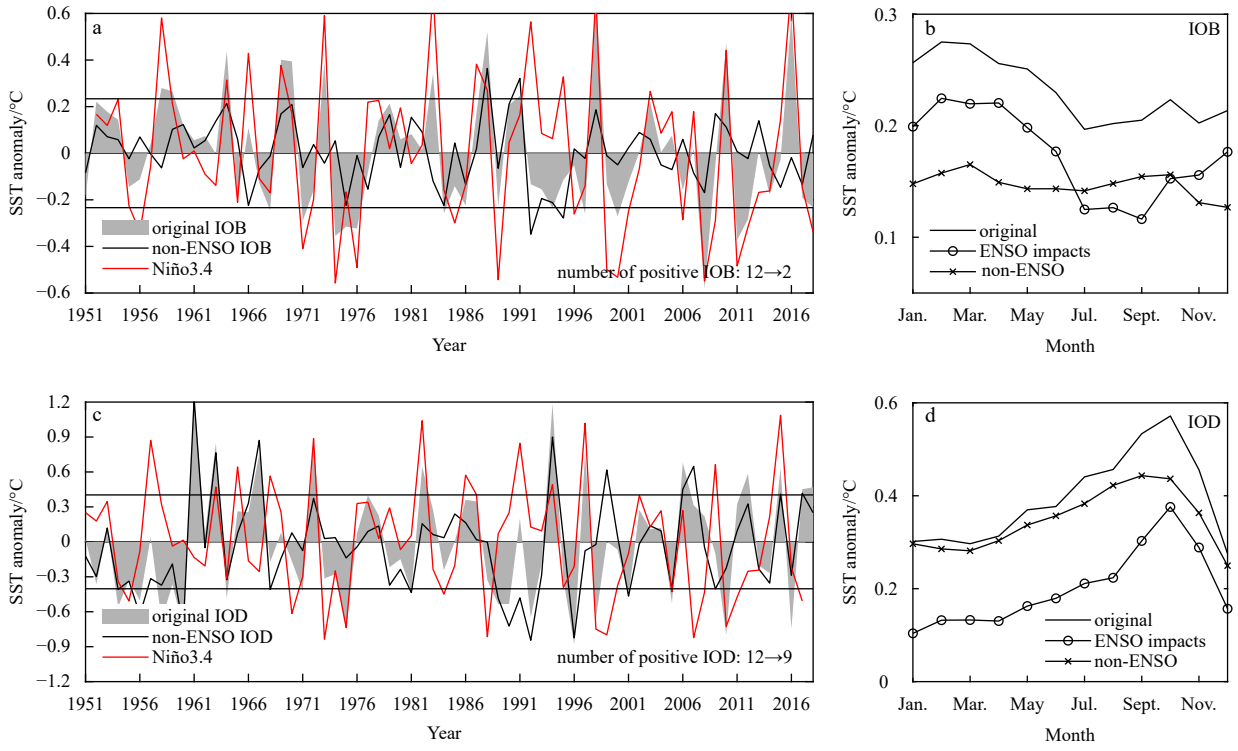

Fig. 4. ENSO impacts on the Indian Ocean Basin (IOB) and Indian Ocean Dipole (IOD) modes. a and c. Trimonthly mean of the IOB (February–April) and the IOD (August–October) indices calculated by original SST anomalies and SST anomalies (grey shading) without the ENSO impacts (black solid line), respectively. The red line represents the Niño3.4 index (December–February) scaled by 1/3 in a and 1/2 in c for better display of the ENSO variability. The red line of a lags that of c by one-year since the IOB and the IOD tend to occur in different stages of the ENSO. b and d. Seasonal evolution of the IOB and the IOD calculated by the monthly RMS of each index, respectively. The solid, circled, and crossed lines represent the results based on original SST anomalies, ENSO-induced SST anomalies and SST anomalies without the ENSO impacts, respectively.

2011, 2013; Jourdain et al., 2016). For example, the positive IOD may induce stronger westerly anomalies in the equatorial Pacific and thus enhance the development of El Niño. In return, the El Niño prompts the IOD via the atmosphere bridge. Such interaction eventually strengthens the IOD developing before the ENSO peak, in which case the IOD and the ENSO act as a catalyst to each other. On the other hand, the IOB can accelerate the phase switch from El Niño to La Niña. The SST warming in the IO induces an atmospheric Kelvin wave that propagates eastward along the equator into the western Pacific, which is known as the Matsuno-Gill pattern (Matsuno, 1966; Gill, 1980). This Kelvin wave induces easterly wind anomalies in the equatorial Pacific,

leading to a following La Niña event that further affects the IO (Xie et al., 2009).

In these senses, the leading and delayed ENSO impacts on the IO SST are both considerable. Evaluation regarding the impacts in each stage can be achieved by retaining one stage impacts and then using it to subtract all-stage removed results (Figs 5 and 6). Two regions, the southeastern tropical IO and the tropical IO, are selected, since they are known as the dominant regions of the IOD and the IOB, respectively (Du et al., 2008, 2013b). Because the concurrent impacts contribute much less to these regions compared with impacts from other two stages as discussed above (Figs 5a and 6a), the leading and delayed ENSO impacts are focused for the following discussions.

Figure 5 shows that both the leading and delayed impacts are influential to the southeastern tropical IO. During the developing year of the El Niño (La Niña), the IO SST anomalies induced by the ENSO impacts cool down (warm up) especially during July to November since the IOD has been preconditioned by the IO summer monsoon and the ENSO starts to develop. These results correspond to Fig. 4d that the ENSO impacts concentrate on the IOD peak season. However, some cooling events persist longer starting from the beginning of the year. Those impacts were remarkable from the 1960s to the 1990s, indicating a decadal variation. The Pacific Decadal Oscillation is a possible reason to the IOD decadal variability through the adjustment of the thermocline depth over the eastern tropical IO during that period (Ummenhofer et al., 2017). On the other hand, the delayed impacts also play a role in the IOD transition, in contrast to the leading impacts that promote the IOD in autumn of the developing year (Fig. 5b). The delayed impacts turn opposite in spring and even persist to winter of the decaying year (Fig. 5c). This is in accord with the fact that the SST over the southeastern tropical IO warms up (cools down) anomalously during the El Niño (La Niña) decaying year and exert influences on the East Asia and northwest Pacific (Huang et al., 2010; Chen et al., 2016, 2018). Overall, as the dominant area of the IOD, the southeastern tropical IO is sensitive to both the leading and delayed ENSO impacts, and hence affects the IOD evolution.

Regarding the tropical IO, the delayed impacts are much stronger than the leading impacts since the IOB usually develops in the ENSO decaying year (Fig. 6). However, the durations of delayed impacts vary in different periods. For example, the strong El Niño event in 1982/83 had a warming effect in the tropical IO in the whole decaying year, while the 1997/98 and 2015/16 events only induced warming in the first several months (Fig. 6c). This difference may also be related to the ENSO decadal variability. The ENSO impacts on the IO SST increased since the 1970s because the ENSO became stronger and persisted longer than the former period, as stronger anticyclonic wind stress curl anomalies excited stronger westward propagating oceanic downwelling Rossby waves in the southern tropical IO, causing stronger anomalous SST warming (Xie et al., 2010). However, even in the post-1970s period, the delayed ENSO impacts underwent different stages. During the 1980s to the mid-1990s, the delayed impacts persisted throughout the year, while those diminished after July since the mid-1990s (Fig. 6c). On the other hand, the decadal variability also seems to operate in the leading impacts, which were stronger during the 1960s to the 1970s over the tropical IO (Fig. 6b).

It is interesting to investigate more about those decadal variations of the ENSO impacts since the ENSO features strong decadal variability (Zhang et al., 1997; Chen and Wallace, 2015). The CLR results show how correlation coefficients vary temporally in the IO when a 12-year running window is applied. Here,

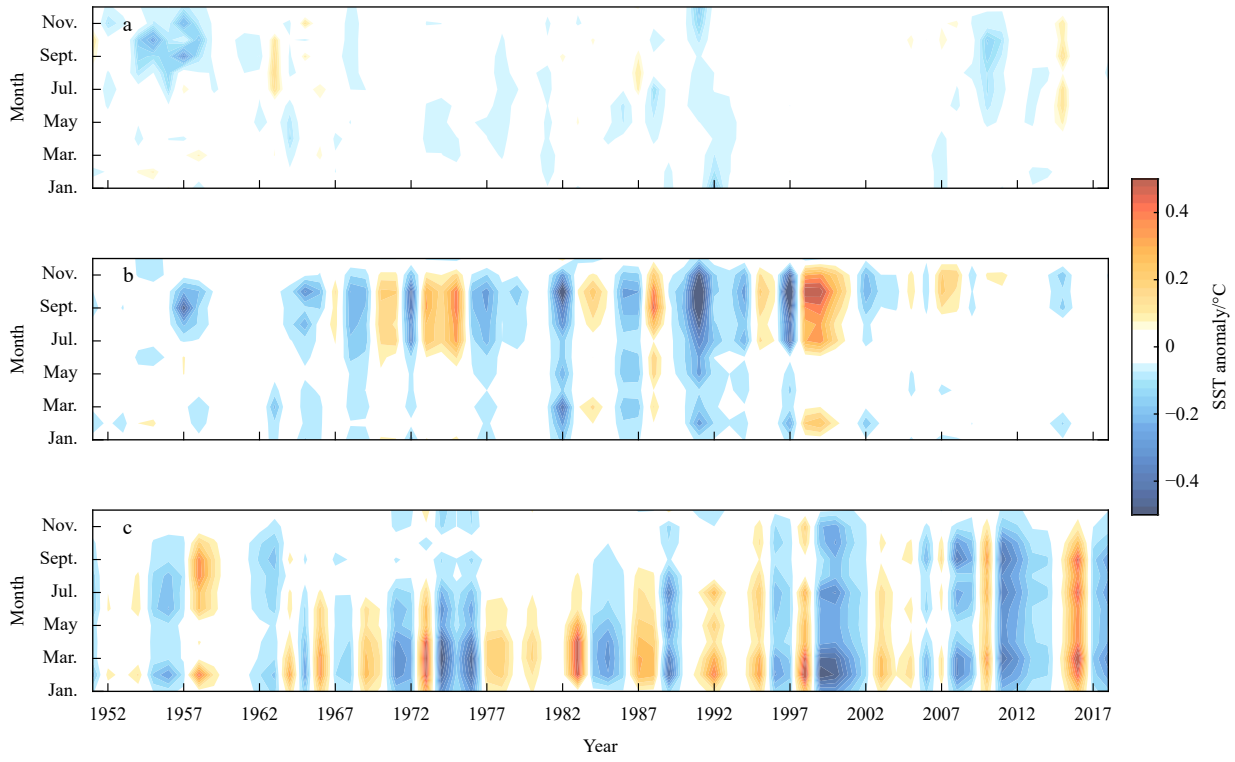

Fig. 5. Isolated ENSO impacts during the ENSO concurrent (a), developing (b), and decaying (c) stages on the area-mean SST anomalies over the southeastern tropical Indian Ocean (10°S–0°, 90°–110°E). All shown results are exceeding the 80% confidence level of students' *t* test applied in the combined linear regression.

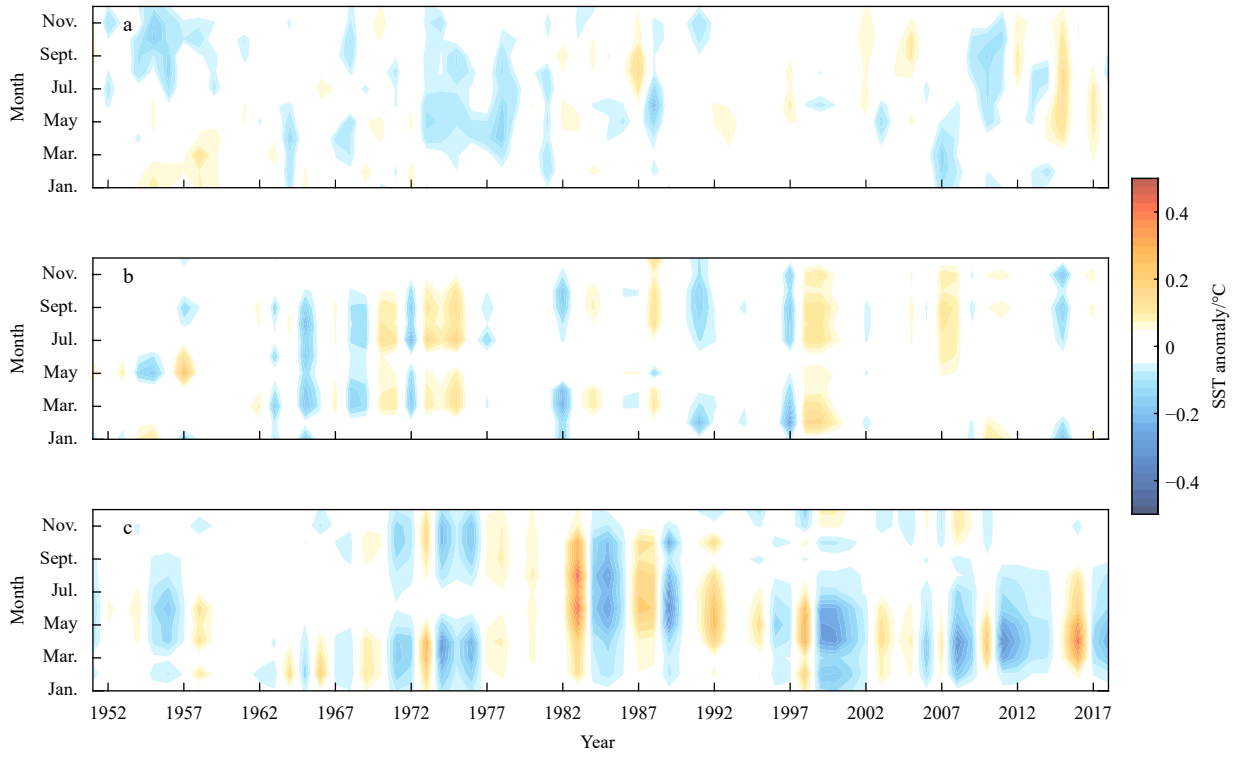

Fig. 6. Isolated ENSO impacts during the ENSO concurrent (a), developing (b), and decaying (c) stages on the area-mean SST anomalies over the tropical Indian Ocean (15°S–15°N, 40°–100°E). All shown results are exceeding the 80% confidence level of students' *t* test applied in the combined linear regression.

the regional-mean SST indices in four regions indicated in Fig. 3c based on higher RMS values of the ENSO-related SST anomalies are chosen. Figure 7 shows the correlations in the ENSO concurrent stage (Fig. 7a), developing stage (September, Fig. 7b), and decaying stage (March, Fig. 7c) of ENSO. Note that the confidence level is set loosely at 80% in the CLR, otherwise the ENSO impacts would considerably remain under the condition of a stricter threshold (e.g., 90% or 95%).

The decadal variations of ENSO impacts are spatiotemporally different (Fig. 7). During the concurrent stage (Fig. 7a), the region west of Australia (Box D) was negatively correlated with the ENSO though it was very weak before the 1980s, while the other regions were positively correlated. Although the western tropical IO (Box A) and the southern IO (Box C) showed similar positive responses, the southeastern tropical IO (Box B) had very weak correlation with the ENSO from the mid-1980s to the mid-2000s. During the ENSO developing stage (Fig. 7b), both Boxes B and D had negative responses to the ENSO especially during the 1970s to the 2000s. However, Boxes A and C were positively correlated with the ENSO, while Box C exhibited decadal variations with stronger responses during the 1970s to the 2000s. During the ENSO decaying year (Fig. 7c), the delayed impacts on Boxes A–C were positively and significantly correlated in the form of the IOB, though the correlations were relatively low during the 1980s; while those were almost negative on Box D. Thus, the decadal variation of the ENSO impacts on the IO is considerable and varied regionally. The CLR including these aspects is expected to provide fairer results on the internal variability research of the IO (Zhang et al., 2020).

The partial regression/correlation analyses are widely used to assess the ENSO impacts on not only the IO but also the globe (Zhou et al., 2010; Cai et al., 2011; Ham et al., 2013; Zhao et al., 2016). Comparably, the partial CLR is tried to obtain the ENSO impacts by setting IOB, IOD and other SST indices as additional predictors in Eq. (1). However, the partial CLR cannot totally isolate the ENSO impacts on the IO SST by including any SST index in the IO, since the IO SST is strongly linked with the ENSO as showed in this study. The partial regression/correlation analyses may be applied only if two climate modes are independent. Therefore, it would be more proper to study the isolated influences of a climate phenomenon besides the ENSO, e.g., the IOD impacts on salinity (Kido and Tozuka, 2017), while it could not work for the ENSO-induced phenomenon like the IOB. To some extent, the CLR adopts a simple but direct regression that may have better performance on removing ENSO impacts.

However, the CLR has its own limitation. For instance, the non-linear effects of the ENSO are hardly captured, which is also a challenge in the climate research (Penland and Matrosova, 2006; Compo and Sardeshmukh, 2010). Although the CLR can partly capture the asymmetry of the ENSO cycle (i.e., La Niña is generally weaker but more frequent than El Niño; Figs 5 and 6), it cannot reflect how the atmosphere responds to SST anomalies with different background SSTs, as the air-sea interaction is more active in a warmer condition. This may be a major shortcoming in the isolation of ENSO impacts. Extension of the CLR based on nonlinear regression techniques, e.g., a sign-separated regression (Cai et al., 2012), may address this issue, and it will be helpful to quantitative assessment of the ENSO contribution to the asymmetry of the IOB and the IOD (Hong et al., 2010).

5 Summary

The present study uses the CLR to revisit the ENSO impacts on the IO SST. The CLR considers the ENSO as a dynamical entity that consists of concurrent, developing, and decaying stages,

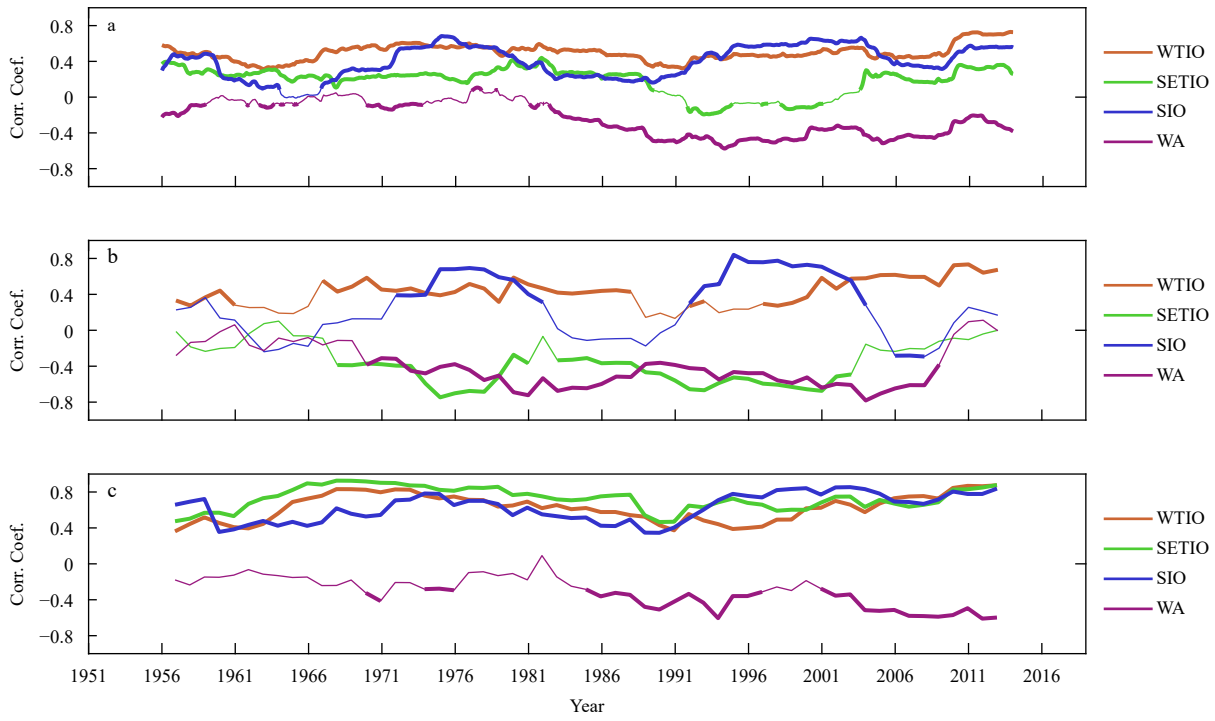

Fig. 7. Decadal variations of the ENSO impacts during the concurrent (a), the developing (b), and the decaying (c) stages. The orange, green, blue, and violet lines indicate the area-mean SST indices over the western TIO (WTIO) (Box A shown in Fig. 3c), the SETIO (Box B shown in Fig. 3c), the southern IO (SIO) (Box C shown in Fig. 3c), and the region west of Australia (WA) (Box D shown in Fig. 3c), respectively. The thick parts are exceeding the 80% confidence level of students' *t* test applied in the combined linear regression.

and that cannot be completely represented by an index (e.g., Niño3.4). By this method, the ENSO impacts are successfully isolated for all and during its each stage. Two climate modes in the IO, the IOB and IOD modes, are used to show how the ENSO induces SST variabilities in the IO. After applying the CLR to remove the ENSO impacts, the results show that the spring peak of the IOB disappears and the number of the IOB events decreases significantly, while the number of events is only slightly reduced and the autumn peak remains for the IOD, indicating that the IOB is more strongly influenced by the ENSO than the IOD (Fig. 8).

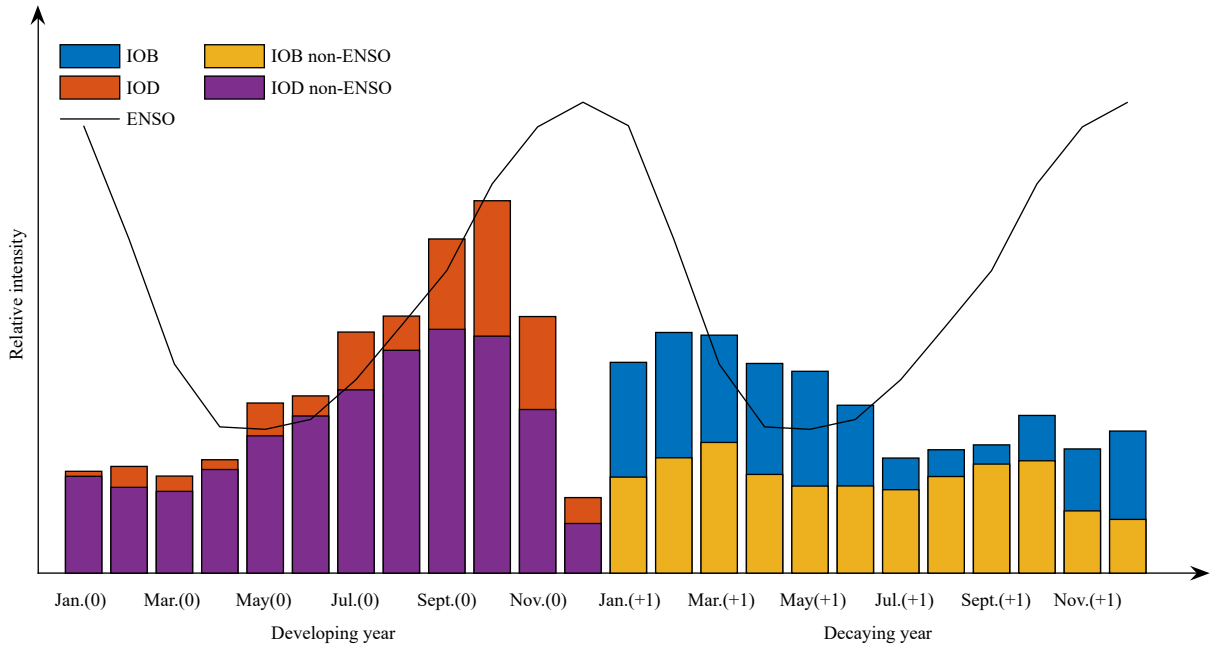

Fig. 8. Schematic diagram of the ENSO impacts on the IOB and the IOD. The black line shows the ENSO intensity derived by the monthly RMS of the Niño3.4 index. The red (blue) and violet (yellow) bars represent the intensity of the IOD (IOB) based on the original SST anomalies and SST anomalies without the ENSO impacts. The developing year and decaying year of ENSO are marked as (0) and (+1), respectively. Note that all the indices are scaled down respectively for better display.

The isolations of impacts from each period reveal that the leading impacts of ENSO are influential to the IOD development, while the delayed impacts urge the IOD phase switch and prompt the IOB development. However, the concurrent impacts influence the IOB and IOD least since the evolution of ENSO is not in phase with these modes. Moreover, the decadal variations of the ENSO impacts are important to study the SST variabilities over different regions in the IO. The CLR would be a helpful method to study the intrinsic variabilities of the IO.

Acknowledgements

We thank two anonymous reviewers for their constructive comments and Jianwei Chi for helpful discussion. We acknowledge the NOAA/OAR/ESRL PSD, Boulder, Colorado, USA, for providing the monthly ERSSTv5 data on their web site at http://www.esrl.noaa.gov/psd/.

References

Abram N J, Gagan M K, Cole J E, et al. 2008. Recent intensification of tropical climate variability in the Indian Ocean. Nature Geoscience, 1(12): 849–853, doi: 10.1038/ngeo357

Alexander M A, Bladé I, Newman M, et al. 2002. The atmospheric bridge: The influence of ENSO teleconnections on air-sea interaction over the global oceans. Journal of Climate, 15(16): 2205–2231, doi: 10.1175/1520-0442(2002)015<2205:TABTIO>2.0.CO;2

Annamalai H, Kida S, Hafner J. 2010. Potential impact of the tropical Indian Ocean–Indonesian Seas on El Niño characteristics. Journal of Climate, 23(14): 3933–3952, doi: 10.1175/2010JCLI3396.1

Annamalai H, Murtugudde R, Potemra J, et al. 2003. Coupled dynamics over the Indian Ocean: spring initiation of the Zonal Mode. Deep Sea Research Part Ⅱ: Topical Studies in Oceanography, 50(12–13): 2305–2330

Annamalai H, Xie Shangping, McCreary J P, et al. 2005. Impact of Indian Ocean sea surface temperature on developing El Nino. Journal of Climate, 18(2): 302–319, doi: 10.1175/JCLI-3268.1

Ashok K, Guan Zhaoyong, Yamagata T. 2001. Impact of the Indian Ocean Dipole on the relationship between the Indian monsoon rainfall and ENSO. Geophysical Research Letters, 28(23): 4499–4502, doi: 10.1029/2001GL013294

Ashok K, Guan Zhaoyong, Yamagata T. 2003. A look at the relationship between the ENSO and the Indian Ocean Dipole. Journal of the Meteorological Society of Japan, 81(1): 41–56, doi: 10.2151/jmsj.81.41

Behera S K, Luo Jingjia, Masson S, et al. 2006. A CGCM study on the interaction between IOD and ENSO. Journal of Climate, 19(9): 1688–1705, doi: 10.1175/JCLI3797.1

Behera S K, Luo Jingjia, Yamagata T. 2008. Unusual IOD event of 2007. Geophysical Research Letters, 35(14): L14S11

Behera S K, Yamagata T. 2001. Subtropical SST dipole events in the southern Indian Ocean. Geophysical Research Letters, 28(2): 327–330, doi: 10.1029/2000GL011451

Behera S K, Yamagata T. 2003. Influence of the Indian Ocean Dipole on the southern oscillation. Journal of the Meteorological Society of Japan, 81(1): 169–177, doi: 10.2151/jmsj.81.169

Bretherton C S, Widmann M, Dymnikov V P, et al. 1999. The effective number of spatial degrees of freedom of a time-varying field. Journal of Climate, 12(7): 1990–2009, doi: 10.1175/1520-0442(1999)012<1990:TENOSD>2.0.CO;2

Cai Wenju, Santoso A, Wang Guojian, et al. 2015. ENSO and greenhouse warming. Nature Climate Change, 5(9): 849–859, doi: 10.1038/nclimate2743

Cai Wenju, Van Rensch P, Cowan T, et al. 2011. Teleconnection pathways of ENSO and the IOD and the mechanisms for impacts on australian rainfall. Journal of Climate, 24(15): 3910–3923, doi: 10.1175/2011JCLI4129.1

Cai Wenju, Van Rensch P, Cowan T, et al. 2012. An asymmetry in the IOD and ENSO teleconnection pathway and its impact on australian climate. Journal of Climate, 25(18): 6318–6329, doi: 10.1175/JCLI-D-11-00501.1

Chen Zesheng, Du Yan, Wen Zhiping, et al. 2018. Indo-Pacific climate during the decaying phase of the 2015/16 El Niño: role of southeast tropical Indian Ocean warming. Climate Dynamics, 50(11–12): 4707–4719

Chen Xianyao, Wallace J M. 2015. ENSO-Like variability: 1900–2013. Journal of Climate, 28(24): 9623–9641, doi: 10.1175/JCLI-D-15-0322.1

Chen Zesheng, Wen Zhiping, Wu Renguang, et al. 2016. Roles of tropical SST anomalies in modulating the western north Pacific anomalous cyclone during strong La Niña decaying years. Climate Dynamics, 49(1–2): 633–647

Chowdary J S, Gnanaseelan C. 2007. Basin-wide warming of the Indian Ocean during El Niño and Indian Ocean dipole years. International Journal of Climatology, 27(11): 1421–1438, doi: 10.1002/joc.1482

Chowdary J S, Patekar D, Srinivas G, et al. 2019. Impact of the Indo-Western Pacific Ocean Capacitor mode on South Asian summer monsoon rainfall. Climate Dynamics, 53(3–4): 2327–2338

Chowdary J S, Xie Shangping, Tokinaga H, et al. 2012. Interdecadal variations in ENSO teleconnection to the Indo–Western Pacific for 1870–2007. Journal of Climate, 25(5): 1722–1744, doi: 10.1175/JCLI-D-11-00070.1

Compo G P, Sardeshmukh P D. 2010. Removing ENSO-related variations from the climate record. Journal of Climate, 23(8): 1957–1978, doi: 10.1175/2009JCLI2735.1

Crétat J, Terray P, Masson S, et al. 2017. Intrinsic precursors and timescale of the tropical Indian Ocean Dipole: insights from partially decoupled numerical experiment. Climate Dynamics, 51(4): 1311–1332

Deser C, Alexander M A, Xie Shangping, et al. 2010. Sea surface temperature variability: patterns and mechanisms. Annual Review of Marine Science, 2: 115–143, doi: 10.1146/annurev-marine-120408-151453

Du Yan, Cai Wenju, Wu Yanling. 2013a. A new type of the Indian Ocean Dipole since the mid-1970s. Journal of Climate, 26(3): 959–972, doi: 10.1175/JCLI-D-12-00047.1

Du Yan, Qu Tangdong, Meyers G. 2008. Interannual variability of sea surface temperature off Java and Sumatra in a global GCM. Journal of Climate, 21(11): 2451–2465, doi: 10.1175/2007JCLI1753.1

Du Yan, Xie Shangping, Huang Gang, et al. 2009. Role of air–sea interaction in the long persistence of El Niño–induced North Indian Ocean warming. Journal of Climate, 22(8): 2023–2038, doi: 10.1175/2008JCLI2590.1

Du Yan, Xie Shangping, Yang Yali, et al. 2013b. Indian Ocean variability in the CMIP5 multimodel ensemble: the Basin Mode. Journal of Climate, 26(18): 7240–7266, doi: 10.1175/JCLI-D-12-00678.1

Du Yan, Yang Lei, Xie Shangping. 2011. Tropical Indian Ocean influence on northwest Pacific tropical cyclones in summer following strong El Niño. Journal of Climate, 24(1): 315–322, doi: 10.1175/2010JCLI3890.1

Du Yan, Zhang Yuhong. 2015. Satellite and Argo observed surface salinity variations in the tropical Indian Ocean and their association with the Indian Ocean dipole mode. Journal of Climate, 28(2): 695–713, doi: 10.1175/JCLI-D-14-00435.1

Feng Ming, McPhaden M J, Xie Shangping, et al. 2013. *La Niña* forces unprecedented Leeuwin Current warming in 2011. Scientific Reports, 3: 1277, doi: 10.1038/srep01277

Fischer A S, Terray P, Guilyardi E, et al. 2005. Two independent triggers for the Indian Ocean Dipole/Zonal mode in a coupled GCM. Journal of Climate, 18(17): 3428–3449, doi: 10.1175/JCLI3478.1

Gill A E. 1980. Some simple solutions for heat-induced tropical circulation. Quarterly Journal of the Royal Meteorological Society, 106(449): 447–462, doi: 10.1002/qj.49710644905

Gnanaseelan C, Vaid B H. 2009. Interannual variability in the Biannual Rossby waves in the tropical Indian Ocean and its relation to Indian Ocean Dipole and El Nino forcing. Ocean Dynamics,

60(1): 27–40
Guan Zhaoyong, Yamagata T. 2003. The unusual summer of 1994 in East Asia: IOD teleconnections. Geophysical Research Letters, 30(10): 1544
Guo Feiyan, Liu Qinyu, Sun S, et al. 2015. Three types of Indian Ocean dipoles. Journal of Climate, 28(8): 3073–3092, doi: 10.1175/JCLI-D-14-00507.1
Ham Y G, Kug J S, Park J Y. 2013. Two distinct roles of Atlantic SSTs in ENSO variability: North Tropical Atlantic SST and Atlantic Niño. Geophysical Research Letters, 40(15): 4012–4017, doi: 10.1002/grl.50729
Han Weiqing, Vialard J, McPhaden M J, et al. 2014. Indian Ocean decadal variability: a review. Bulletin of the American Meteorological Society, 95(11): 1679–1703, doi: 10.1175/BAMS-D-13-00028.1
Hong C C, Li T, LinHo, et al. 2010. Asymmetry of the Indian Ocean basinwide SST anomalies: roles of ENSO and IOD. Journal of Climate, 23(13): 3563–3576, doi: 10.1175/2010JCLI3320.1
Horii T, Hase H, Ueki I, et al. 2008. Oceanic precondition and evolution of the 2006 Indian Ocean Dipole. Geophysical Research Letters, 35(3): L03607
Huang Gang, Hu Kaiming, Xie Shangping. 2010. Strengthening of tropical Indian Ocean teleconnection to the Northwest Pacific since the mid-1970s: an atmospheric GCM study. Journal of Climate, 23(19): 5294–5304, doi: 10.1175/2010JCLI3577.1
Huang Boyin, Thorne P W, Banzon V F, et al. 2017. Extended reconstructed sea surface temperature, version 5 (ERSSTv5): upgrades, validations, and intercomparisons. Journal of Climate, 30(20): 8179–8205, doi: 10.1175/JCLI-D-16-0836.1
Izumo T, Vialard J, Lengaigne M, et al. 2010. Influence of the state of the Indian Ocean Dipole on the following year's El Niño. Nature Geoscience, 3(3): 168–172, doi: 10.1038/ngeo760
Jourdain N C, Lengaigne M, Vialard J, et al. 2016. Further insights on the influence of the Indian Ocean Dipole on the following year's ENSO from observations and CMIP5 models. Journal of Climate, 29(2): 637–658, doi: 10.1175/JCLI-D-15-0481.1
Kennedy J J, Rayner N A, Smith R O, et al. 2011a. Reassessing biases and other uncertainties in sea surface temperature observations measured in situ since 1850: 1. Measurement and sampling uncertainties. Journal of Geophysical Research: Atmospheres, 116(D14): D14103, doi: 10.1029/2010JD015218
Kennedy J J, Rayner N A, Smith R O, et al. 2011b. Reassessing biases and other uncertainties in sea surface temperature observations measured in situ since 1850: 2. Biases and homogenization. Journal of Geophysical Research: Atmospheres, 116(D14): D14104, doi: 10.1029/2010JD015220
Kido S, Tozuka T. 2017. Salinity variability associated with the positive Indian Ocean Dipole and its impact on the upper ocean temperature. Journal of Climate, 30(19): 7885–7907, doi: 10.1175/JCLI-D-17-0133.1
Klein S A, Soden B J, Lau N C. 1999. Remote sea surface temperature variations during ENSO: evidence for a tropical atmospheric bridge. Journal of Climate, 12(4): 917–932, doi: 10.1175/1520-0442(1999)012<0917:RSSTVD>2.0.CO;2
Kug J S, Li T, An S I, et al. 2006. Role of the ENSO–Indian Ocean coupling on ENSO variability in a coupled GCM. Geophysical Research Letters, 33(9): L09710
Lau N C, Nath M J. 2004. Coupled GCM simulation of atmosphere-ocean variability associated with zonally asymmetric SST changes in the tropical Indian Ocean. Journal of Climate, 17(2): 245–265, doi: 10.1175/1520-0442(2004)017<0245:CGSOAV>2.0.CO;2
Luo Jingjia, Behera S, Masumoto Y, et al. 2008. Successful prediction of the consecutive IOD in 2006 and 2007. Geophysical Research Letters, 35(14): L14S02
Luo Jingjia, Zhang Ruochao, Behera S K, et al. 2010. Interaction between El Niño and extreme Indian Ocean Dipole. Journal of Climate, 23(3): 726–742, doi: 10.1175/2009JCLI3104.1
Masumoto Y, Meyers G. 1998. Forced Rossby waves in the southern tropical Indian Ocean. Journal of Geophysical Research: Oceans, 103(C12): 27589–27602, doi: 10.1029/98JC02546
Matsuno T. 1966. Quasi-geostrophic motions in the equatorial area. Journal of the Meteorological Society of Japan, 44(1): 25–43, doi: 10.2151/jmsj1965.44.1_25
McPhaden M J, Yu Xuri. 1999. Equatorial waves and the 1997-98 El Niño. Geophysical Research Letters, 26(19): 2961–2964, doi: 10.1029/1999GL004901
Meehl G A. 1993. A coupled air-sea biennial mechanism in the tropical Indian and Pacific regions: role of the ocean. Journal of Climate, 6(1): 31–41, doi: 10.1175/1520-0442(1993)006<0031:ACASBM>2.0.CO;2
Morioka Y, Tozuka T, Yamagata T. 2012. How is the Indian Ocean Subtropical Dipole excited?. Climate Dynamics, 41(7–8): 1955–1968
Park H S, Chiang J C H, Lintner B R, et al. 2010. The delayed effect of major El Niño events on Indian monsoon rainfall. Journal of Climate, 23(4): 932–946, doi: 10.1175/2009JCLI2916.1
Penland C, Matrosova L. 2006. Studies of El Niño and interdecadal variability in tropical sea surface temperatures using a nonnormal filter. Journal of Climate, 19(22): 5796–5815, doi: 10.1175/JCLI3951.1
Qiu Yun, Cai Wenju, Guo Xiaogang, et al. 2014. The asymmetric influence of the positive and negative IOD events on China's rainfall. Scientific Reports, 4: 4943
Rasmusson E M, Carpenter T H. 1982. Variations in tropical sea surface temperature and surface wind fields associated with the Southern Oscillation/El Niño. Monthly Weather Review, 110(5): 354–384, doi: 10.1175/1520-0493(1982)110<0354:VITSST>2.0.CO;2
Reynolds R W, Rayner N A, Smith T M, et al. 2002. An improved in situ and satellite SST analysis for climate. Journal of Climate, 15(13): 1609–1625, doi: 10.1175/1520-0442(2002)015<1609:AIISAS>2.0.CO;2
Saji N H, Goswami B N, Vinayachandran P N, et al. 1999. A dipole mode in the tropical Indian Ocean. Nature, 401(6751): 360–363
Santoso A, England M H, Cai Wenju. 2012. Impact of Indo-Pacific feedback interactions on ENSO dynamics diagnosed using ensemble climate simulations. Journal of Climate, 25(21): 7743–7763, doi: 10.1175/JCLI-D-11-00287.1
Schott F A, Xie Shangping, McCreary J P Jr. 2009. Indian Ocean circulation and climate variability. Reviews of Geophysics, 47(1): RG1002
Smith T M, Reynolds R W, Peterson T C, et al. 2008. Improvements to NOAA's historical merged land–ocean surface temperature analysis (1880–2006). Journal of Climate, 21(10): 2283–2296, doi: 10.1175/2007JCLI2100.1
Stuecker M F, Timmermann A, Jin Feifei, et al. 2017. Revisiting ENSO/Indian Ocean Dipole phase relationships. Geophysical Research Letters, 44(5): 2481–2492, doi: 10.1002/2016GL072308
Sun Shuangwen, Lan Jian, Fang Yue, et al. 2015. A triggering mechanism for the Indian Ocean Dipoles independent of ENSO. Journal of Climate, 28(13): 5063–5076, doi: 10.1175/JCLI-D-14-00580.1
Suzuki S, Behera S K, Iizuka S, et al. 2004. Indian Ocean subtropical dipole simulated using a coupled general circulation model. Journal of Geophysical Research: Oceans, 109(C9): C09001
Tozuka T, Kataoka T, Yamagata T. 2014. Locally and remotely forced atmospheric circulation anomalies of Ningaloo Niño/Niña. Climate Dynamics, 43(7–8): 2197–2205
Ummenhofer C C, Biastoch A, Böning C W. 2017. Multidecadal Indian Ocean variability linked to the Pacific and implications for preconditioning Indian Ocean Dipole events. Journal of Climate, 30(5): 1739–1751, doi: 10.1175/JCLI-D-16-0200.1
Vinayachandran P N, Saji N H, Yamagata T. 1999. Response of the equatorial Indian Ocean to an unusual wind event during 1994. Geophysical Research Letters, 26(11): 1613–1616, doi: 10.1029/1999GL900179
Wang Hui, Murtugudde R, Kumar A. 2016. Evolution of Indian Ocean Dipole and its forcing mechanisms in the absence of ENSO. Climate Dynamics, 47(7–8): 2481–2500
Wang Chuanyang, Xie Shangping, Kosaka Y. 2020. ENSO-unrelated variability in Indo–northwest Pacific climate: regional coupled

ocean–atmospheric feedback. Journal of Climate, 33(10): 4095–4108, doi: 10.1175/JCLI-D-19-0426.1

Webster P J, Moore A M, Loschnigg J P, et al. 1999. Coupled ocean-atmosphere dynamics in the Indian Ocean during 1997–98. Nature, 401(6751): 356–360, doi: 10.1038/43848

Xie Shangping, Annamalai H, Schott F A, et al. 2002. Structure and mechanisms of South Indian Ocean climate variability. Journal of Climate, 15(8): 864–878, doi: 10.1175/1520-0442(2002)015<0864:SAMOSI>2.0.CO;2

Xie Shangping, Du Yan, Huang Gang, et al. 2010. Decadal shift in El Niño influences on Indo–western Pacific and East Asian climate in the 1970s. Journal of Climate, 23(12): 3352–3368, doi: 10.1175/2010JCLI3429.1

Xie Shangping, Hu Kaiming, Hafner J, et al. 2009. Indian Ocean capacitor effect on Indo–western Pacific climate during the summer following El Niño. Journal of Climate, 22(3): 730–747, doi: 10.1175/2008JCLI2544.1

Xie Shangping, Kosaka Y, Du Yan, et al. 2016. Indo-western Pacific ocean capacitor and coherent climate anomalies in post-ENSO summer: A review. Advances in Atmospheric Sciences, 33(4): 411–432, doi: 10.1007/s00376-015-5192-6

Xie Shangping, Philander S G H. 1994. A coupled ocean-atmosphere model of relevance to the Itcz in the eastern Pacific. Tellus A: Dynamic Meteorology and Oceanography, 46(4): 340–350, doi: 10.3402/tellusa.v46i4.15484

Xu Jianjun, Chan J C L. 2001. The role of the Asian–australian monsoon system in the onset time of El Niño events. Journal of Climate, 14(3): 418–433, doi: 10.1175/1520-0442(2001)014<0418:TROTAA>2.0.CO;2

Yang Jianling, Liu Qinyu, Xie Shangping, et al. 2007. Impact of the Indian Ocean SST basin mode on the Asian summer monsoon. Geophysical Research Letters, 34(2): L02708

Yang Yun, Xie Shangping, Wu Lixin, et al. 2015. Seasonality and predictability of the Indian Ocean Dipole mode: ENSO forcing and internal variability. Journal of Climate, 28(20): 8021–8036, doi: 10.1175/JCLI-D-15-0078.1

Yu Jinyi, Mechoso C R, McWilliams J C, et al. 2002. Impacts of the Indian Ocean on the ENSO cycle. Geophysical Research Letters, 29(8): 46–1

Yuan Dongliang, Wang Jing, Xu Tengfei, et al. 2011. Forcing of the Indian Ocean Dipole on the interannual variations of the tropical Pacific Ocean: roles of the Indonesian throughflow. Journal of Climate, 24(14): 3593–3608, doi: 10.1175/2011JCLI3649.1

Yuan Dongliang, Zhou Hui, Zhao Xia. 2013. Interannual climate variability over the tropical Pacific Ocean Induced by the Indian Ocean Dipole through the indonesian throughflow. Journal of Climate, 26(9): 2845–2861, doi: 10.1175/JCLI-D-12-00117.1

Zhang Lianyi, Du Yan, Cai Wenju. 2018a. A spurious positive Indian Ocean Dipole in 2017. Science Bulletin, 63(18): 1170–1172, doi: 10.1016/j.scib.2018.08.001

Zhang Lianyi, Du Yan, Cai Wenju. 2018b. Low-Frequency variability and the unusual Indian Ocean Dipole events in 2015 and 2016. Geophysical Research Letters, 45(2): 1040–1048, doi: 10.1002/2017GL076003

Zhang Lianyi, Du Yan, Cai Wenju, et al. 2020. Triggering the Indian Ocean Dipole from the southern hemisphere. Geophysical Research Letters, 47: e2020GL088648

Zhang Lei, Han Weiqing, Li Yuanlong, et al. 2018c. Mechanisms for generation and development of the Ningaloo Niño. Journal of Climate, 31(22): 9239–9259, doi: 10.1175/JCLI-D-18-0175.1

Zhang Yuan, Wallace J M, Battisti D S. 1997. ENSO-like interdecadal variability: 1900–93. Journal of Climate, 10(5): 1004–1020, doi: 10.1175/1520-0442(1997)010<1004:ELIV>2.0.CO;2

Zhao Xia, Yuan Dongliang, Yang Guang, et al. 2016. Role of the oceanic channel in the relationships between the basin/dipole mode of SST anomalies in the tropical Indian Ocean and ENSO transition. Advances in Atmospheric Sciences, 33(12): 1386–1400, doi: 10.1007/s00376-016-6048-4

Zheng Xiaotong, Xie Shangping, Du Yan, et al. 2013. Indian Ocean Dipole response to global warming in the CMIP5 multimodel ensemble. Journal of Climate, 26(16): 6067–6080, doi: 10.1175/JCLI-D-12-00638.1

Zhou Liantong, Tam C Y, Zhou Wen, et al. 2010. Influence of South China Sea SST and the ENSO on winter rainfall over South China. Advances in Atmospheric Sciences, 27(4): 832–844, doi: 10.1007/s00376-009-9102-7